Topology regulates the distribution pattern of excitations in excitable dynamics on graphs

Mark Müller-Linow,[1] Carsten Marr,[1] and Marc-Thorsten Hütt[2]
[1]*Bioinformatics Group, Department of Biology, Darmstadt University of Technology, 64287 Darmstadt, Germany*
[2]*School of Engineering and Science, International University Bremen, 28759 Bremen, Germany*
(Received 27 October 2005; published 19 July 2006)

We study the average excitation density in a simple model of excitable dynamics on graphs and find that this density strongly depends on certain topological features of the graph, namely connectivity and degree correlations, but to a lesser extent on the degree distribution. Remarkably, the average excitation density is changed via the distribution pattern of excitations: An increase in connectivity induces a transition from globally to locally organized excitations and, as a result, leads to an increase in the excitation density. A similar transition can be induced by increasing the rate of spontaneous excitations while keeping the graph architecture constant.

DOI: 10.1103/PhysRevE.74.016112 PACS number(s): 89.75.Hc, 05.45.Tp

I. INTRODUCTION

Global topological properties of networklike systems have been discussed intensely in the past few years and, moreover, provided a unifying perspective on a large variety of biological and technical networks [1–5]. Particularly for biological networks, observed topological features are compared with those obtained with specific algorithms of graph generation with the aim of, ultimately, specifying the evolutionary principles behind an observed network architecture. Beyond the level of topology, a huge interest of recent research lies in dynamic processes on graphs. The key question is how topological features induce dynamic function. Fields of research range from genetic networks (see, e.g., [6–8]) to neural networks [9,10], reaction-diffusion processes on graphs [11,12], as well as more general forms of dynamics [13–16]. Epidemic models are particularly suitable to study the influence of topological aspects such as the degree distribution and degree correlations. In recent years, the susceptible-infected-susceptible (SIS) [17–19] and the susceptible-infected-removed/recovered (SIR) [17,20–22] models have been analyzed; however, most of the investigations are targeting the infection rate and the epidemic threshold of a system [19,23–25], while there exist only few results concerning the stability of dynamic patterns (i.e., the *distribution* of excitations) and the emergence and interrelation of global and local excitation as a function of graph architecture [26]. Methods from dynamical systems theory and particularly from synchronization theory may in the long run be highly useful for understanding the forms of dynamic organization resulting from architectural features of the system. The crucial question from this pattern-driven perspective is, how are excitations stored in a network and how do features of this storage pattern change with graph topology?

In this paper, we address the relation between the global properties of dynamics on a graph and the topological features characterizing the graph by studying a specific model of signal propagation and biological pattern formation, namely the forest fire (FF) model [27,28]. This formulation of an excitable medium, which can be implemented on a graph with arbitrary architecture, helps to understand how such excitations propagate in a system with complex architecture and, consequently, how information is processed by such a system. The version discussed here has been introduced by Drossel and Schwabl [28], who studied it as a model system of self-organized criticality. Here, we will analyze the model in a parameter regime, where on a regular (two-dimensional) lattice propagating waves are observed. Mathematically, this model is a cellular automaton with stochastic elements. It consists of three discrete states for each node (fire F, tree T, empty site E), which are updated synchronously in discrete time steps according to the following rules: (i) A tree becomes a burning tree, if there is at least one fire in its direct neighborhood; if not, accidental ignition occurs with the lightning probability f; (ii) a fire becomes an empty site; (iii) a tree regenerates ($E \rightarrow T$) with growth probability p. These three states, T, F, and E, correspond the excitable (susceptible), excited, and refractory states, respectively, of a generic excitable system. In spite of the choice of the specific model, we study generic excitable dynamics on graphs in order to understand how topological properties influence the distribution and statistics of excitations. Due to the generic sequence of states inscribed in the model—excitable $\rightarrow$ excited $\rightarrow$ refractory $\rightarrow$ excitable—that a node undergoes, this formal model investigation basically has two fields of applications: (i) aspects of neural information processing and (ii) certain variants of epidemic dynamics. The parallel to epidemic dynamics becomes apparent, when one looks at the SIRS model [26], which is a slightly changed version of the SIR model. In this model system, the recovered state is able to switch over to the susceptible state, ensuring persistent signal propagation in contrast to the SIR model.

In order to quantify the relevance of graph topology, we use different elementary graph types with variable connectivity. Our aim is to show that the connectivity of a graph plays a pivotal role for the excitation density in the system regardless of the degree distribution itself.

II. RESULTS

We investigated three typical graph architectures, namely (i) the random (ER) graph, introduced by Erdös and Rényi [29], which is constructed by randomly adding links to a given set of unconnected nodes. The ER graph is characterized by a Poissonian degree distribution, i.e., every node has

about the same degree. (ii) The link-added (WS) graph, introduced by Watts and Strogatz [30–32] in the context of the small-world model analysis. The WS graph consists of a given ring lattice with N nodes and $m=N$ links, together with additional randomly added links. Depending on the connectivity, the degree distribution shows ER graph characteristics and, additionally, a high proportion of small degrees. (iii) The scale-free (BA) graph, introduced by Barabási and Albert [33]. Our generation algorithm of the BA graph starts with a complete graph connectivity of m_0 nodes. A typical value of m_o is 2 or 3. In each iterative step, a new node is added to the graph and connected with m links to the nodes with the highest degrees preferentially. The probability of linkage is proportional to the degree of a node, and neither self-links nor double links are allowed. In order to obtain continuous values of connectivity z, we used noninteger numbers of m. This value constitutes a certain probability that the upper next integer number is used instead of m at each iteration step. We checked that details of the graph generation algorithm within the general BA framework do not essentially change our results. Such a network has a power-law degree distribution with few highly connected nodes (hubs) and a vast number of sparsely linked nodes.

According to the specific graph generation algorithm, networks with $N=1000$ and varying connectivities were generated [ER graphs $10^{-4}<z<1$, WS graph, and BA graph $2\times10^{-3}<z<1$, where $z=2m/N(N-1)$ and m is the number of links]. In the following, T, F, and E denote the number of trees, fires, and empty sites; the corresponding state densities are ρ_T, ρ_F, and ρ_E.

No analytical result of the forest fire model for the described graph architectures with variable connectivity has been obtained so far, but an early salient theoretical approach to the FF model was the mean-field analysis of the steady-state densities [34,35], which can be extended to yield approximate expressions for the fire density ρ_F as a function of connectivity, as well as features of the fire distribution on the graph. Let us assume that in each time step, the k neighboring nodes are selected randomly and update rules are applied synchronously. Obviously, neither correlations between nodes nor degree correlations occur in such a network, since the number of neighbors is always k. The number of fires, trees, and empty sites at time $t+1$ can be derived from the update rules with the lightning and growth probabilities f and p and the mean number of neighbors k,

$$F(t+1) = fT(t) + kT(t)\theta_F(t), \tag{1}$$

$$T(t+1) = (1-f)T(t) + pE(t) - kT(t)\theta_F(t), \tag{2}$$

$$E(t+1) = F(t) + (1-p)E(t), \tag{3}$$

where θ_F is the probability to find a fire as a neighbor of a tree. Here, we evaluate this general mean-field model in order to obtain an expression for the excitation density ρ_F. For small fire densities, higher-order contributions can be neglected and the probability θ_F is simply given by the fire density $\rho_F(t)=F(t)/N$. The steady-state solution for ρ_F can be found by multiplying the above equations with $1/N$ (in order to pass from absolute numbers to state densities), setting $\rho(t+1)=\rho(t)$, and using the subsidiary condition $1=\rho_F+\rho_T+\rho_E$. While both solutions of the quadratic equations for ρ_F constitute stable fixed points, only one of them yields positive values for the fire densities. With the connectivity z and $n=N-1$, this solution can be written as

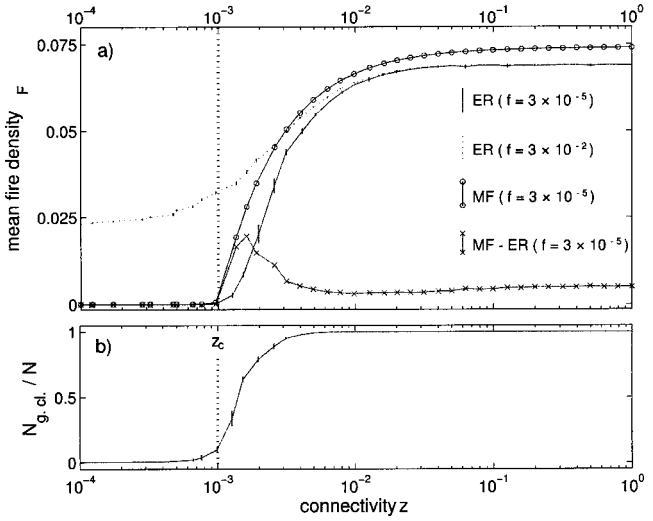

FIG. 1. (a) Connectivity z dependency of the mean fire density $\langle\rho_F\rangle$ for random graphs [simulated results (ER) and mean-field approximation (MF) with $f=3\times10^{-5}$ ($f=3\times10^{-2}$) and $p=0.08$]. The MF-ER curve depicts the deviation between analytical and simulated results. The maximal deviation around $z=1.5\times10^{-5}$ indicates the connectivity where the m/n ratio of the giant cluster exceeds 1. (b) ER graph percolation represented by the relative size of the largest connected cluster $N_{\mathrm{g.cl.}}$ and the percolation threshold z_c.

$$\rho_F = \frac{nzp - f - p - fp + \sqrt{-4nzp^2 + (f+p+fp+nzp)^2}}{2nz(1+p)}. \tag{4}$$

This mean-field approach is widely used to understand the properties of the FF model run on d-dimensional lattices [36]. However, it is by construction a much better approximation for the case of ER graphs, where the degree deviations around a mean degree k are small and degree correlations are absent. What is known about the synchronization of excitations in such a system? On lattices of sufficiently high N, global synchronized excitation events are nonexistent. A regular structure without shortcuts and a high network diameter favor the formation of propagating waves, thus leading to a persistent level of excitations.

For $p \gg f$ we argue that the parameter p affects primarily the overall time scale of the dynamics. Therefore, we tested different parameter settings and confirmed the assumption that over a wide range of p the overall proportions of excitation patterns are marginally influenced and ρ_F simply scales with p. In the following, we used two parameter settings ($p=0.08$, $f_1=3\times10^{-5}$, $f_2=3\times10^{-2}$) in order to test the f dependence of the excitation patterns. The length $t_{\max}$ of each simulation was 25000 updates; 10 simulations were performed for each network-parameter constellation. In Fig. 1(a), the mean fire density $\langle\rho_F\rangle$ is plotted as a function of the

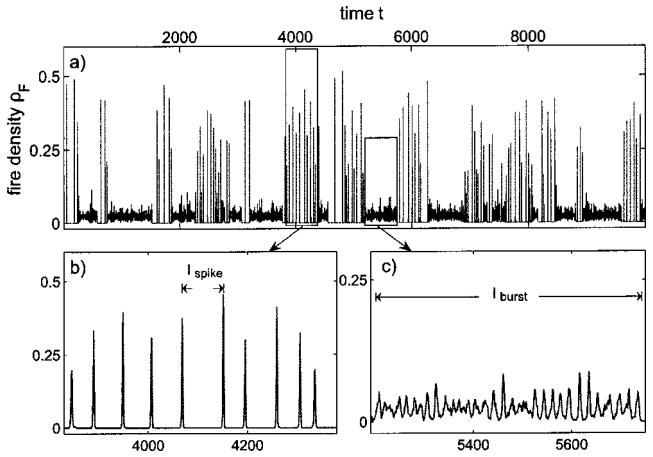

FIG. 2. (a) Time series of the fire density ρ_F of a random graph ($z=0.006$; $N=1000$) with $f=3\times10^{-5}$ and $p=0.08$. Sections display the typical dynamical behavior, namely (b) the spike regimes, where l_{spike} is the duration between two adjoining spike events and (c) the burst regimes, where l_{burst} is the duration of a burst.

connectivity z for both the simulated and the analytical results. For the interpretation of these results, percolation effects have to be taken into account, i.e., the phenomenon that in the ER model the transition from an unconnected to a connected graph with increasing connectivity takes place via a large connected subset (giant component) surrounded by small unconnected fragments emerging in the graph. At a certain connectivity, this component comprises the whole graph. The ER graph percolation was determined by computing the size of the giant cluster [Fig. 1(b)]. The theoretical percolation threshold is given by $z_c=1/N$ [1]. As one can see from the difference between the numeric simulation and the analytical result in Fig. 1, the analytical result shows a comparatively increased excitation density right above z_c. The phase transition at this threshold, where a giant component appears in the system, is already incorporated by the steady-state model [$\rho_F\to0$ for $z\to z_C$ in Eq. (4)]. Therefore, this deviation cannot be explained by percolation effects. A closer look at the time series of the simulations for low z reveals two regions that differ fundamentally in their excitation patterns [Fig. 2(a)]. The first regime exhibits very short and strong excitations (spikes), which can be interpreted as globally coinciding events [Fig. 2(b)], while in the second regime long-lasting density fluctuations (bursts) with clearly reduced intensity occur as a result of local consecutive coinciding events [Fig. 2(c)].

When averaged over time, the fire density in the spike regime is considerably smaller than for bursts. It is given by the mean distance between two spikes l_{spike} [Fig. 2(b)] and the mean number of trees burned in one spike event. From Eq. (4), one can see that the overall excitation in a sparsely connected graph ($z<z_c$) with $f\ll p$ depends mainly on the parameter f, thus explaining the increase of $\langle\rho_F\rangle$ for $f_2=3\times10^{-2}$. In a graph with no connections and small lightning probability f, the density $\langle\rho_F\rangle$ matches f. In the limit of infinite system sizes and $z=1$, Eq. (4) can be simplified to $\rho_F=\frac{p}{1+p}$. Both limiting values agree numerically with the asymptotics of the corresponding curve in Fig. 1(a).

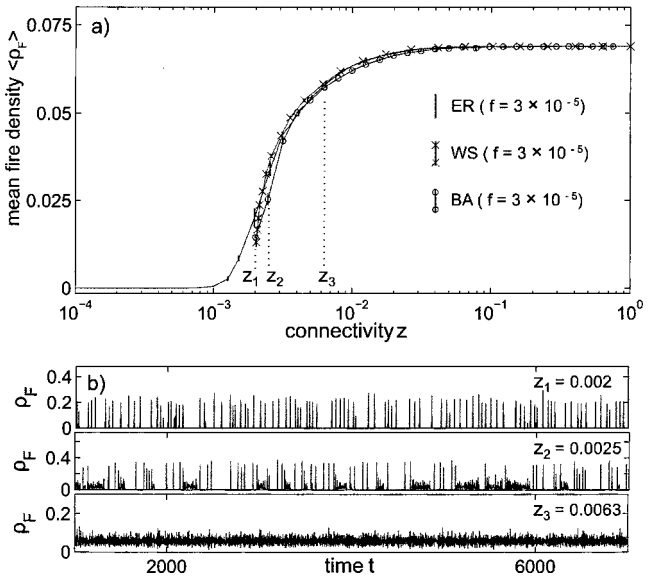

FIG. 3. (a) Connectivity z dependence of the mean fire density $\langle\rho_F\rangle$ for three different graph types: random graph (ER), scale-free graph (BA), and link-added graph (WS) with $f=3\times10^{-5}$ and $p=0.08$. (b) Sections of time series of fire density ρ_F of the BA graph for different connectivities. For the smallest value of z, i.e., $z_1=0.002$, excitation is solely induced by spike dynamics; for values above $z_3=0.0063$, burst dynamics prevails. The transition region in between shows both excitation patterns of varying ratio, e.g., for $z_2=0.0025$.

In order to study the relation of the connectivity dependence and percolation effects, we compared simulation results of the BA and WS graphs with the ER graph results. Figure 3(a) shows the plots for all three graph types for $p=0.08$ and $f=3\times10^{-5}$. Surprisingly, all curves show similar transitions of ρ_F above the percolation threshold z_c. Figure 3(b) shows segments of the time series for three different values of z of the BA graph. The time series $z=0.002$ contains only spike regimes, the time series $z=0.063$ has only a burst regime, and the one in the transition region $z=0.0025$ is characterized by the coexistence of spike and burst regimes. Thus, a change in z induces a change in the distribution pattern of excitations and, as a result, in the entire excitation density. The similarity of the three curves constitutes an unexpectedly marginal influence of the degree distribution on the excitation density. The degree distribution is the most important distinctive characteristic of these three graph topologies. However, in regulating the average amount of excitations within the graph, it only plays a minor role.

To confirm this scenario of an increased ρ_F due to a qualitative change in the distribution pattern of excitations, we quantified the excitation density of the burst regimes for the BA graph as a function of connectivity and compared it with the mean fire density $\langle\rho_F\rangle$ (Fig. 4). For further comparison, the excitation density of the burst regimes in an ER graph was added. The similarity in curve forms suggests that the excitation strength is a direct consequence of the proportion of global and local coincidences, i.e., at the switch from spikes to bursts. Additionally, the low-z behavior can be interpreted in a similar form: Results for the ER graph support

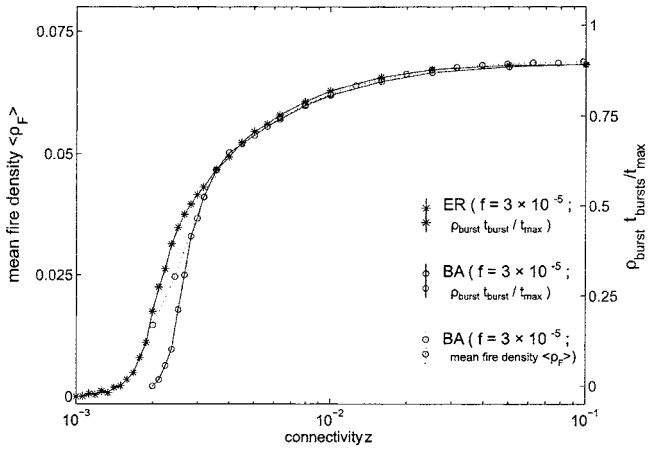

FIG. 4. The integrated excitation density in the burst regime $\rho_{\mathrm{burst}}t_{\mathrm{burst}}/t_{\max}$ depending on connectivity z for the ER graph and the BA graph (solid lines) compared to the results of the mean fire density $\langle\rho_F\rangle$ of the ER graph (dashed line).

the idea that a giant cluster is able to produce bursts even below the threshold of $z=0.002$, where a connected BA graph is formed, and for this reason contributes more to the excitation strength than expected from the overall connectivity. This leads to a shift (toward lower z values) at the corresponding curve in Fig. 4.

Results for different lightning probabilities f in the ER graph studies [see Fig. 1(a)] suggest that f is influencing the distribution of excitations in a likewise manner as the network connectivity. Therefore, we repeated the simulations for the three different graph architectures (ER, BA, and WS, each with $N=1000$), this time keeping the graph connectivity and the growth probability constant at $z=0.006$ and $p=0.02$, respectively, while varying the lightning probability in the range of $10^{-7}<f<1$. Figure 5(a) depicts the results for the mean fire density $\langle\rho_F\rangle$ of these simulations (25000 updates, 10 runs for each network-parameter constellation). The distinct transition to higher ρ_F under the increase of spontaneous excitations is induced by a shift in the distribution pattern of excitations from spike to burst dynamics [see Fig. 5(b)], which has also been observed in the topological induced transition (Fig. 3). A difference between both transitions is the plateaulike behavior at intermediate values of f. In this regime, the excitation density $\langle\rho_F\rangle$ is almost independent of f, and only at even higher values of f is a further increase of $\langle\rho_F\rangle$ seen. The limiting factor in this range of intermediate f is the number of trees: A constant $\langle\rho_F\rangle$ suggests that, on average, any node spontaneously excited within a time step would also be excited by an excitation in the immediate neighborhood. Increasing p reduces this plateau regime (data not shown), as expected from this argument.

Raising the control parameter f is comparable to an increase of the connectivity. By adding links to a network [31,37], as in the generation rule for WS graphs, shortcuts are generated that are able to transport excitations to subparts of the network, which were not accessible before. From the perspective of the region in the graph, to which the shortcut leads, this corresponds to accidental excitations, quite similar

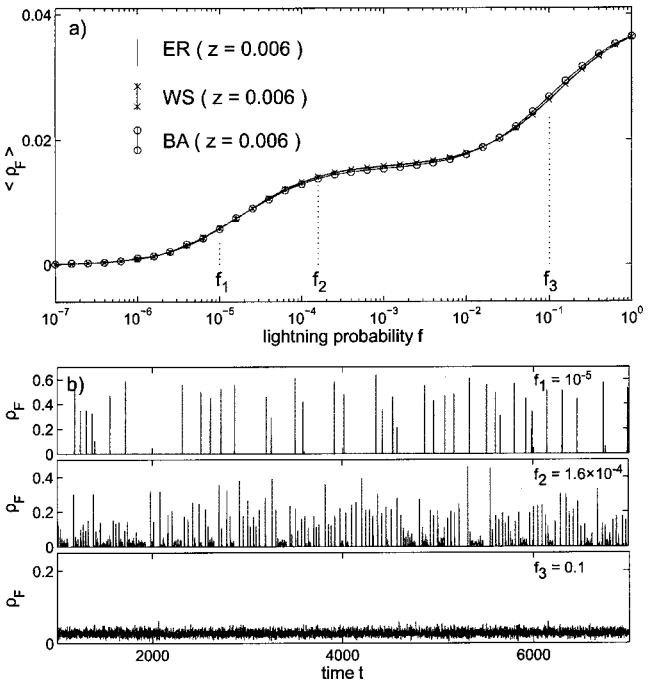

FIG. 5. (a) Lightning probability f dependence of the mean fire density $\langle\rho_F\rangle$ for three different graph architectures: random graph (ER), scale-free graph (BA), and link-added graph (WS) with connectivity $z=0.006$ and $p=0.02$. (b) Sections of time series of fire density ρ_F of the BA graph for different lightning probabilities. Corresponding to the effects of the connectivity z (as shown in Fig. 3), small values of f, e.g., $f_1=3\times10^{-5}$, induce weak excitations caused by a single spike regime; for values above $f=0.01$ predominant burst dynamics cause the highest excitations (see $f_3=0.1$). In between are excitation patterns showing both regimes of varying ratio, e.g., for $f_2=1.6\times10^{-4}$.

to the spontaneous excitations governed by f. The general similarity between shortcuts and noise has also been studied in [38]. Therefore, an increase in the parameter f results in a shift toward burst dynamics especially for low connectivities and in a $\langle\rho_F\rangle$ enhancement at the same time.

The type of distribution pattern depends on the availability of excitable nodes (i.e., nodes in the T state) and on the interval between two excitation incidents. The closer these events are, the more likely is the formation of a burst, because the system possesses a high quantity of refractory nodes E. Within burst events, simultaneous excitation is achieved only in parts of the network; fractions of nodes in state E are regenerated and are thus accessible for excitation during the next time step. The maintenance of locally and simultaneously excited parts leads to a signal persistent in time. The essential topological feature to produce a burst in the FF model seems to be the availability of loops, i.e., sequences of links connecting a node with itself. This characteristic is only possible in networks with $m/N\geqslant1$. At a connecticity level of $z=0.002$, which is the lower boundary for a connected graph at $N=1000$, the BA and WS graphs do not possess any loops (except for a trivial systemwide loop), and are therefore only able to produce spike events. In ER graphs, the topological properties of the giant cluster play an important role for the formation of a burst. In a giant cluster,

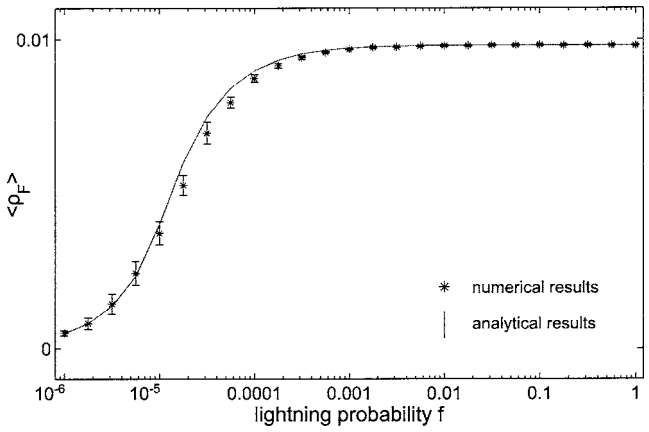

FIG. 6. Numerical and analytical results for the f-dependent fire density $\langle \rho_F \rangle$ in a complete graph ($N=500$).

the ratio of links and nodes exceeds 1 for even smaller values of z, thus producing bursts and explaining the elevation of $\langle \rho_F \rangle$ (ER) for low connectivities and, moreover, explaining the point of the largest deviation between ER graph simulation and the mean-field approximation, which lies between z_c and $z=0.002$ [Fig. 1(a)].

We extended our analytical approach to the FF model for complete graphs. A detailed description is given in Appendix A. With this groundwork it is possible to evaluate the fire density ρ_F and the proportion of the respective dynamical regimes (e.g., the temporal fraction of the burst regimes a_{burst}) for each constellation of the lightning probability f and the tree growth probability p [see Eqs. (A3) and (A4)]. We compared the analytical results for a complete graph ($N=500$, $p=0.01$, and $10^{-6}<f<1$) with the corresponding numerical results from simulations (25000 updates with 25 runs for each parameter constellation). This comparison is illustrated in Fig. 6 with the computation of the mean fire density $\langle \rho_F \rangle$. The comparative analysis of a_{burst} (data not shown) yields a similar result. Despite small variations, the analyses predict the simulated results very well and may thus serve as a basis for further studies of the FF model on graph architectures with variable connectivity and degree correlations.

As a second topological property, we investigated the influence of degree correlations on the dynamical behavior. To alter the degree correlations, we used a method of Trusina *et al.* [39], who introduced a concept to distinguish between hierarchical and antihierarchical networks. For this investigation, scale-free networks are best suited because they show a broad degree distribution. In our investigations, we find a distinct shift toward higher ρ_F with increasing antihierarchization, especially in the transition region of ρ_F (data not shown). As stated before, an increase of ρ_F results from a proportionate enhancement of the burst regimes. During antihierarchization, hubs are continuously separated from each other by nodes with small degrees, thus increasing the diameter and the modularity of the whole network at the same time. As a consequence, parts of the network show an increased connectivity compared to their neighborhood and are thus able to produce bursts on a local level. In contrast to this, hierarchized networks are characterized by linked hubs and treelike chains of nodes. The ability to produce bursts is reduced to the densely linked center of the network, while spike behavior is comparatively enhanced. These topological differences are more noticeable the more sparsely the network is connected, resulting in the largest deviations of the fire density ρ_F for different values of k_A at the same time.

III. DISCUSSION

We have demonstrated that the forest fire model is in principle capable of exhibiting two forms of distribution pattern of excitations on graphs, namely bursts and series of spikes. These patterns are characterized by different excitation storing capacities. Thus, the transition from low to high excitation densities is accompanied by a transition in the excitation patterns. This switch to high excitation densities (and, correspondingly, from one excitation pattern to the other) can be triggered topologically (by increasing the network's connectivity) or dynamically (by increasing the probability of spontaneous excitations).

In a recent study of coupled integrate-and-fire neurons, a similar transition from spikes to a burstlike regime of persistent excitations has been related to the functioning of the working memory [9], and in an epidemiological study of the SIRS model the increase of the excitation density with connectivity is explained by phase transition to global synchronization [26].

The crucial influence of the connectivity of a network on the excitation density is accompanied by topological effects of higher order, the degree correlations, which are reflected in modular properties, while the degree distribution seems to play a subordinate role in this context.

In biological systems, the ability to produce a recurrent distribution pattern of excitations may contribute to function, resulting in a link between functional properties and structural features. In a certain sense, a process may dynamically integrate groups of nodes to form dynamical (nonstationary) modules (burst behavior) within the given topological framework of the graph. It would be interesting to see if (and under which conditions) such dynamical modules coincide with topological modules and, furthermore, if such an explicit exploitation of topology by dynamics may even enhance dynamical features, such as the amount of excitations stored within a graph.

APPENDIX A: PROBABILISTIC CALCULATION OF THE FIRE DENSITY

Here, we derive probabilistic expressions for the analytical calculation of the fire density, as shown in Fig. 6 for a complete graph. As in the main text, the forest-fire dynamics is well defined by the tree growth probability p, the lightning probability f, and the system size N.

We first consider the extreme case of $f=1$, where every growing tree burns immediately. The overall fire density ρ_F is determined by the average number of growing trees in one time step, $\bar{T}=p\bar{E}$, where $\bar{E}$ is the average number of empty sites in the system. This quantity differs from N by existing trees (which is $p\bar{E}$) and already burning sites (again $p\bar{E}$), $\bar{E}=N-2\bar{E}p$. Therefore,

$$\bar{E} = \frac{N}{1+2p} \tag{A1}$$

and the average fire density is given by

$$\rho_F(f=1) = \frac{p\bar{E}}{N} = \frac{p}{1+2p}. \tag{A2}$$

Note that the corresponding time series may comprise cases in which no trees grow at all and the fire extinguishes.

For $f \neq 1$, the time series is made up of bursts and spikes. To calculate the fire density ρ_F for a given parameter set (N,p,f), we have to account for both dynamical regimes,

$$\rho_F = a_{\text{spike}}\rho_{\text{spike}} + a_{\text{burst}}\rho_{\text{burst}}, \tag{A3}$$

where ρ_x is the fire density in the regime x and a_x is the proportion of the respective regime in the total time series. We define this quantity by

$$a_{\text{burst}} = \frac{l_{\text{burst}}}{l_{\text{burst}} + Sl_{\text{spike}}} = 1 - a_{\text{spike}}, \tag{A4}$$

where l_{burst} is the typical burst length, l_{spike} is the typical separation of two spikes, and S is the mean number of consecutive spikes in a typical time series [see Figs. 2(b) and 2(c)].

In the remainder of this appendix, we restrict our derivations to complete graphs, i.e., graphs with connectivity $z=1$, where every node is connected to all other nodes in the network. This is an approximation to general topologies, but nonetheless a worthwhile case study, where salient features of the mixture of bursts and spikes can be thoroughly understood.

The number of fires in the burst regime on complete graphs equals the number of growing trees under the condition that at least one tree grows in every time step, so that the burst proceeds. The probability for a burst to stop equals the probability that no trees grow on the empty sites in one time step, $P_{\text{stop}}=(1-p)^{\bar{E}}$. Including the conditional probability $1/(1-P_{\text{stop}})$ and Eq. (A2), the fire density in the burst regime reads

$$\rho_{\text{burst}} = \frac{1}{1-(1-p)^{\bar{E}}}\frac{p}{1+2p}. \tag{A5}$$

The probability for a burst of length l is given by $(1-P_{\text{stop}})^{l-1}P_{\text{stop}}$. The first moment of this distribution is the average burst length. With Eq. (A1) follows

$$l_{\text{burst}} = P_{\text{stop}}^{-1} = (1-p)^{-N/(1+2p)}. \tag{A6}$$

Both quantities are independent of f.

In the spike regime, lightning ignites a tree that ignites a large part of the system in the next time step. The principal time scale is the typical separation of two spikes, l_{spike}. This quantity clearly incorporates the mean waiting time for a spark t_{spark} on a growing forest.

The number of growing trees in one time step follows a binomial distribution. The mean number of trees to grow on E empty sites in one time step is Ep. The mean number of grown trees after t time steps can be recursively determined, $\bar{T}(t)=\bar{T}(t-1)+p[N-\bar{T}(t-1)]$, and equals

$$\bar{T}(t) = N - [N - T(0)](1-p)^t. \tag{A7}$$

Therein, $T(0)$ is the number of trees in the first time step after a burst or spike has stopped. [After a burst, the mean number of growing trees equals $p(N-\bar{E})=Np\frac{1+p}{1+2p}$.] The probability for no lightning to occur in a system with T trees is $(1-f)^T$. Lightning at time t implies that one of the trees present at $t-1$ has been ignited. Thus the probability P_{spark} for lightning at time $t=1$ is $P_{\text{spark}}(1)=1-(1-f)^{T(0)}$; for $t\geqslant 2$ it follows that $P_{\text{spark}}(t)=(1-f)^{\sum_{\tau=0}^{t-2}\bar{T}(\tau)}[1-(1-f)^{\bar{T}(t-1)}]$. The mean waiting time for lightning to occur in a growing forest is

$$t_{\text{spark}} = \sum_{t=1}^{\infty} tP_{\text{spark}}(t). \tag{A8}$$

The average distance between two spikes in a complete graph is

$$l_{\text{spike}} = t_{\text{spark}} + 2, \tag{A9}$$

where one time step each for the ignition of the graph and the complete burning has to be added by hand. For simplicity, we only regard the spike case where the fire dies out again after two time steps. The average number of fires in a spike equals the number of grown-up trees at time t_{spark} when the lightning ignites the first fire. For the fire density in the whole regime it follows with Eqs. (A8) and (A9) that

$$\rho_{\text{spike}} = \frac{F_{\text{spike}}}{N}\frac{1}{l_{\text{spike}}} = \frac{\bar{T}(t_{\text{spark}})}{N}\frac{1}{l_{\text{spike}}}. \tag{A10}$$

To fully determine the spike regime properties, we need to know the number of spikes in a row. The condition for consecutive spikes is that no trees grow on the empty sites E during the ignition of the graph. The corresponding probability is

$$P_{\text{spike}} = (1-p)^{E(t_{\text{spark}})} = (1-p)^{N-\bar{T}(t_{\text{spark}})}, \tag{A11}$$

The mean number of spikes between two bursts can then be calculated by

$$S = \sum_{s=1}^{\infty} sP_{\text{spike}}^{s-1}(1-P_{\text{spike}}) = \frac{1}{1-P_{\text{spike}}}. \tag{A12}$$

Plugging the above expressions into Eq. (A3) yields the fire density for every parameter set on a complete graph.

[1] R. Albert and A.-L. Barabási, Rev. Mod. Phys. **74**, 47 (2002).
[2] M. E. J. Newman, SIAM Rev. **45**, 167 (2003).
[3] R. Milo, S. Itzkovitz, N. Kashtan, R. Levitt, S. Shen-Orr, I. Ayzenshtat, M. Sheffer, and U. Alon, Science **303**, 1538 (2004).
[4] R. Guimerà and L. N. Amaral, Nature (London) **433**, 895 (2005).
[5] A.-L. Barabási and Z. N. Oltvai, Nat. Rev. Genet. **5**, 101 (2004).
[6] S. Kauffman, C. Peterson, B. Samuelsson, and C. Troein, Proc. Natl. Acad. Sci. U.S.A. **100**, 14796 (2003).
[7] T. I. Lee *et al.*, Science **298**, 799 (2002).
[8] S. Bornholdt, Science **310**, 449 (2005).
[9] A. Roxin, H. Riecke, and A. Solla, Phys. Rev. Lett. **92**, 198101 (2004).
[10] B. Percha, R. Dzakpasu, M. Zochowski, and J. Parent, Phys. Rev. E **72**, 031909 (2005).
[11] L. K. Gallos and P. Argyrakis, Phys. Rev. Lett. **92**, 138301 (2004).
[12] L. K. Gallos and P. Argyrakis, Phys. Rev. E **72**, 017101 (2005).
[13] Y. Bar-Yam and I. Epstein, Proc. Natl. Acad. Sci. U.S.A. **101**, 4341 (2004).
[14] L. A. N. Amaral, A. Díaz-Guilera, A. A. Moreira, A. L. Goldberger, and L. A. Lipsitz, Proc. Natl. Acad. Sci. U.S.A. **101**, 15551 (2004).
[15] C. Marr and M.-T. Hütt, Physica A **354**, 641 (2005a).
[16] M.-T. Hütt and U. Lüttge, Physica A **350**, 207 (2004).
[17] N. T. J. Bailey, *The Mathematical Theory of Infectious Diseases and Its Applications* (Hafner Press, New York, 1975).
[18] R. Pastor-Satorras and A. Vespignani, Phys. Rev. Lett. **86**, 3200 (2001).
[19] R. Pastor-Satorras and A. Vespignani, Phys. Rev. E **63**, 066117 (2001).
[20] R. M. Anderson and R. M. May, *Infectious Diseases of Humans* (Oxford University Press, Oxford, 1991).
[21] H. W. Hethcote, SIAM Rev. **42**, 599 (2000).
[22] Y. Moreno, R. Pastor-Satorras, and A. Vespignani, Eur. Phys. J. B **26**, 521 (2002).
[23] V. Eguíluz and K. Klemm, Phys. Rev. Lett. **89**, 108701 (2002).
[24] M. E. J. Newman, Phys. Rev. E **66**, 016128 (2002).
[25] C. Moore and M. E. J. Newman, Phys. Rev. E **61**, 5678 (2000).
[26] M. Kuperman and G. Abramson, Phys. Rev. Lett. **86**, 2909 (2001).
[27] P. Bak, K. Chen, and C. Tang, Phys. Lett. A **147**, 297 (1990).
[28] B. Drossel and F. Schwabl, Phys. Rev. Lett. **69**, 1629 (1992).
[29] P. Erdös and A. Rényi, Publ. Math. (Debrecen) **6**, 290 (1959).
[30] D. J. Watts and S. H. Strogatz, Nature (London) **393**, 440 (1998).
[31] M. E. J. Newman, C. Moore, and D. J. Watts, Phys. Rev. Lett. **84**, 3201 (2000).
[32] S. H. Strogatz, Nature (London) **410**, 268 (2001).
[33] A.-L. Barabási and R. Albert, Science **286**, 509 (1999).
[34] K. Christensen, H. Flyvbjerg, and Z. Olami, Phys. Rev. Lett. **71**, 2737 (1993).
[35] M. Barthélemy, A. Barrat, R. Pastor-Satorras, and A. Vespignani, J. Theor. Biol. **235**, 275 (2004).
[36] H. J. Jensen, *Self-Organized Criticality* (Cambridge University Press, Cambridge, 1998).
[37] I. Graham and C. C. Matthai, Phys. Rev. E **68**, 036109 (2003).
[38] C. Marr and M.-T. Hütt, Phys. Lett. A **349**, 302 (2006).
[39] A. Trusina, S. Maslov, P. Minnhagen, and K. Sneppen, Phys. Rev. Lett. **92**, 178702 (2004).